Research Article | Vol. 32, No. 20 / 23 Sep 2024 / Optics Express 35678
Optics EXPRESS

Diffractive microoptics in porous silicon oxide by grayscale lithography

LEANDER SIEGLE,[1,*] DAJIE XIE,[2,3] COREY A. RICHARDS,[2,3] PAUL V. BRAUN,[2,3] AND HARALD GIESSEN[1]

[1]4th Physics Institute and Research Center SCoPE, University of Stuttgart, Pfaffenwaldring 57, 70569 Stuttgart, Germany
[2]Department of Materials Science and Engineering, University of Illinois Urbana-Champaign, Urbana, Illinois 61801, USA
[3]Materials Research Laboratory, University of Illinois Urbana-Champaign, Urbana, Illinois 61801, USA
[*]l.siegle@pi4.uni-stuttgart.de

Abstract: We demonstrate focusing as well as imaging using diffractive microoptics, manufactured by two-photon polymerization grayscale lithography (2GL), that have been 3D printed into porous silicon oxide. While typical doublet lens systems require support structures that hold the lenses in place, our optics are held by the porous media itself, decreasing both the fabrication time and design constraints while increasing the optically active area. Compared to the typical two-photon polymerization fabrication process, 2GL offers better shape accuracy while simultaneously increasing throughput. To showcase 2GL manufactured optics in porous media, we fabricate singlet diffractive lenses with a diameter of 500 µm and numerical apertures of up to 0.6. We measure the intensity distribution in the focal plane, and along the optical axis. Furthermore, we design and fabricate a doublet lens system for imaging purposes with a diameter of 600 µm and thinner than 60 µm. We examine the imaging performance with a USAF 1951 resolution test chart and determine the resolution to be 287 lp/mm. 3D printing in porous SiO_2 thus holds great promise for future complex and unconventional microoptical solutions.

1. Introduction

As the third pillar of fabrication apart from subtractive and formative techniques, the additive manufacturing method of two-photon polymerization (2PP) 3D printing has been a growing technology for the fabrication of microoptics and photonics over the last years [1–3]. 2PP has been utilized to manufacture a multitude of optical parts, from typical refractive lenses [4–6] and diffractive optical elements [7,8] to photonic crystals [9,10] and polarization optics [11]. Furthermore, 3D printed microoptics enable applications ranging from micro-needles and endoscopy in biomedicine [12–14] to quantum technology [15–17] and photonic networks [18,19]. The usual drawback of 3D printed microoptics are long fabrication times, which can easily reach times of a day for larger elements [6]. For more complex designs, such as lens stacks, some of the printing time and design effort needs to be utilized to produce supporting structures that hold the optical elements in place. We dramatically reduce the fabrication time to 2 minutes per lens by utilizing diffractive lens designs together with two-photon polymerization grayscale lithography (2GL). With 2GL, we are able to increase the distance between printed layers while preserving the typical shape-accuracy and smoothness, reducing manufacturing times further [20,21]. Additionally, performing 3D printing inside a porous medium eases the need for supporting structures, enabling efficient volumetric integration of complex optics design [19,22,23].

#538142 https://doi.org/10.1364/OE.538142
Journal © 2024 Received 31 Jul 2024; revised 11 Sep 2024; accepted 11 Sep 2024; published 18 Sep 2024

Optics EXPRESS

We demonstrate singlet and doublet diffractive lenses for focusing and imaging that are rapidly manufactured by 2GL. The lenses with diameters in the half-millimeter range are embedded in a 60 µm film of porous SiO_2 ($PSiO_2$), allowing to omit supporting structures typically necessary to anchor structures, especially lens stacks to the substrate [17,21,24]. We first highlight the capability of diffractive lenses fabricated in $PSiO_2$ with simple singlet lenses with four different numerical apertures (NAs) from 0.15 to 0.60. They show close to diffraction limited performance in focusing Gaussian light beams with a wavelength of 600 nm. In the second part we highlight an imaging optical system consisting of two diffractive lenses. This doublet lens with a physical diameter of 600 µm and optical diameter of 575 µm offers high resolution imaging in a thin form factor, as it also fits in the 60 µm thick $PSiO_2$ film.

2. Singlet diffractive focusing lenses

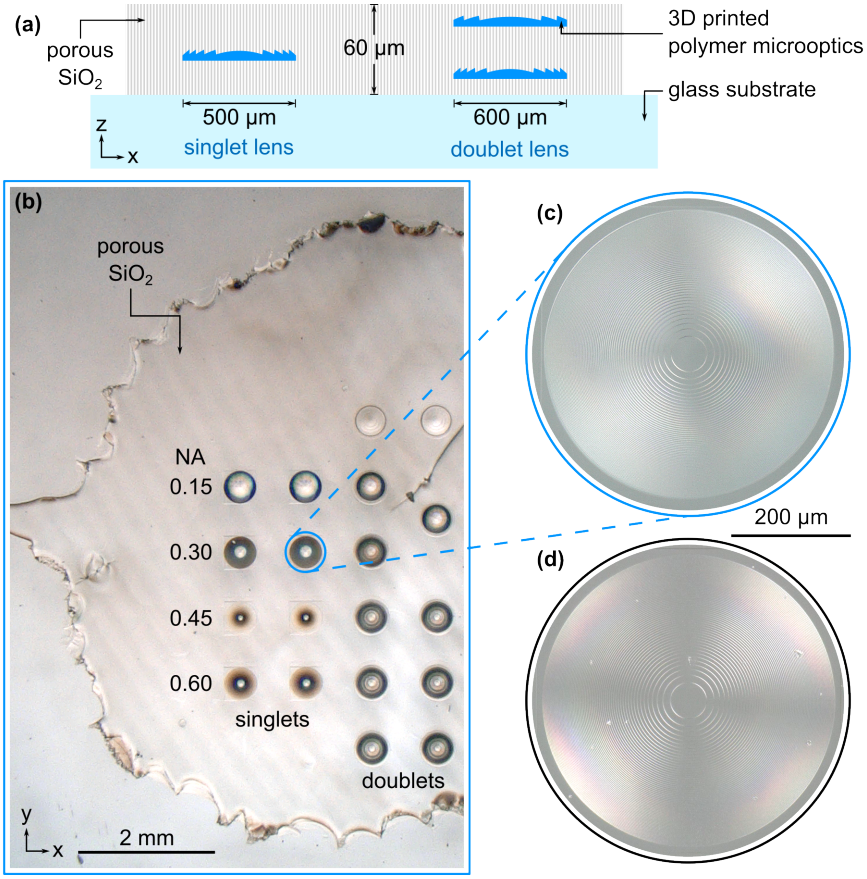

Fig. 1. (a) Schematic side view of singlet and doublet diffractive elements 3D printed into $PSiO_2$ (not to scale). (b) Top-view optical microscopy images of several diffractive microlenses in a 60 µm thick $PSiO_2$ film with physical diameters of 500 µm and 600 µm. The image depicts that we printed each lens twice. The porous medium does not affect the repeatability. (c) Zoom-in of one diffractive singlet lens with a diameter of 500 µm and an NA of 0.3 printed in the $PSiO_2$ film exhibiting the individual Fresnel zones. (d) Diffractive lens fabricated on a glass substrate with the same design parameters as the lens in (c).

To first test the capabilities of 2GL fabricated diffractive optics in $PSiO_2$, we design and print four different singlet lenses with a diameter of 500 µm and numerical apertures of 0.15, 0.30,

Optics EXPRESS

0.45 and 0.60. We use the ray-optical design software Zemax OpticStudio 20.1. The basic layout of the optical system is sketched in Fig. 1(a), with light traveling along the z-axis. The diffractive lens is defined as a binary2-surface located 10 µm below the surface of the 60 µm thick $PSiO_2$ film. With the refractive indices of the lens n_{lens} and of the surrounding medium n_{medium} as well as the design wavelength $\lambda = 600$ nm, the height is given as

$$z(r) = \frac{\lambda}{2\pi(n_{\text{lens}} - n_{\text{medium}})} \text{mod} \left(\sum_{m=1}^{M} a_{2m} r^{2m}, 2\pi \right). \quad (1)$$

Here, a_{2m} are the term numbers that give the optimal phase and M the maximum order to which the parameters are optimized. In case of the singlet lenses, the maximum order M is 20, while the phase will approach a parabolic shape during optimization of the term parameters. The diffractive singlet lenses have spatial frequencies of up to 250 mm^{-1}, 500 mm^{-1}, 750 mm^{-1} and 1000 mm^{-1} at the edge of the lenses with NA's 0.15, 0.30, 0.45, and 0.60. This results in spatial extents of the outmost Fresnel zones of 4 µm, 3 µm, 2 µm, and 1 µm. The refractive index of the polymerized photoresist IP-n162 in $PSiO_2$ is derived using Maxwell-Garnett theory [25]. As the porosity of $PSiO_2$ is 68.29%, the diffractive lens will, to 68.29%, consist of polymerized IP-162 with a refractive index of 1.6221 at the design wavelength of 600 nm [26], while the other 31.71% are made up of $PSiO_2$. Air-filled $PSiO_2$ has a refractive index of 1.1394 at 600 nm, with low dispersion [22]. These values result in an effective refractive index of the polymerized IP-n162 in $PSiO_2$ of 1.5714 at 600 nm, used to define the shape of the lens. The designed height of each Fresnel zone given by Eq. (1) is circa 1.389 µm.

The diffractive lenses are depicted in the two columns on the left of Fig. 1(b) in ascending numerical aperture from top to bottom. A zoom-in of the 0.30 NA lens is illustrated in Fig. 1(c), which highlights all diffractive zones and shows some aliasing due to the resolution of the image. Additionally, we fabricate the 0.30 NA lens on top of a microscopy glass slide, with the same design and fabrication parameters as the one inside $PSiO_2$. The zoom-in of this lens is depicted in Fig. 1(d) and compares well in the shape and look to the lens fabricated in $PSiO_2$. The remaining difference in appearance can be explained by the increased refractive index difference between at the interfaces of the resist IP-n162 and air to IP-n162 and $PSiO_2$.

2.1. Optical performance

To examine the focusing ability of the 3D printed singlet lenses, we use the setup illustrated in Fig. 2(a). Laser light (NKT SuperK Extreme) at a wavelength of 600 nm, filtered by an Acousto-Optic Tunable Filter (NKT SuperK Select+, specified full width at half maximum 2.5-8.5 nm in the visible), is collimated by a triplet fiber collimator (Thorlabs PAF2-A4A) and strikes a pinhole with a diameter of 500 µm, matching the designed aperture of our 3D printed singlet lenses. The sample as seen in Fig. 1(b) is situated on a piezo-electric z-stage (P-736 PI nano Z) that can be moved with high accuracy. The laser is subsequently focused by the printed lens and analyzed by a basic microscopy setup consisting of a 0.7 NA, 60x magnification microscope objective (Nikon CFI S Plan Fluor 60x ELWD MRH08630), a tube lens and a camera (Allied Vision GC2450C). To measure the 3D intensity distribution, an image is taken in steps of 0.1 µm for the entire traveling range of 200 µm. The normalized intensity cross sections in the xy-focal plane and along the optical axis as a zy-plot for the four different types of singlet are depicted in Fig. 2(b). Here, the measurements depicts compact and symmetric Gaussian-shaped focal spots. Small artifacts in the intensity from the fabrication and diffractive nature of the lenses are visible for the two lower NA lenses with NA's of 0.15 and 0.30 but vanish almost completely for the higher NA lenses with NA's 0.45 and 0.60. To quantize the focusing performance, we fit Gaussian profiles through the intensity maximum of the focus along all three spatial axes. The full width at half maximum (FWHM) of the Gaussian profiles depict a symmetric behavior in

Optics EXPRESS

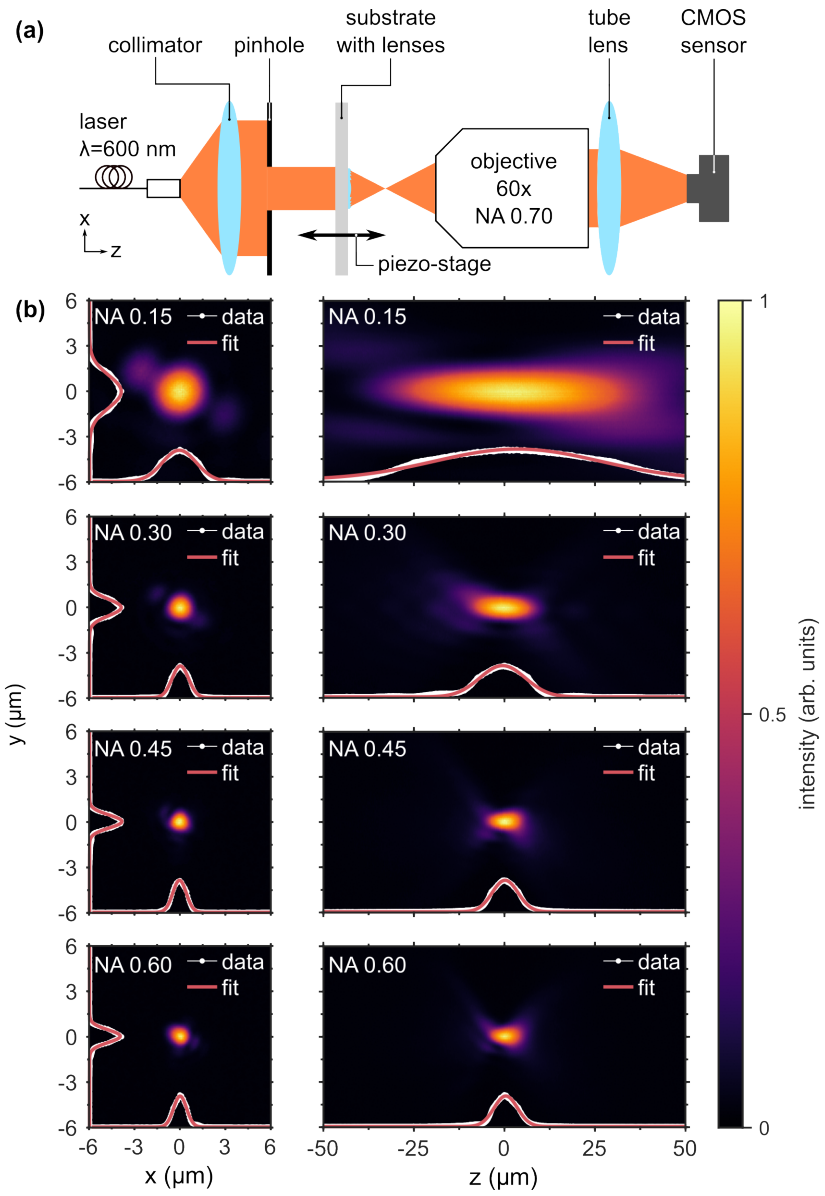

Fig. 2. Focusing performance analysis of the singlet diffractive lenses with numerical apertures of 0.15, 0.30, 0.45, and 0.60. (a) Setup to measure the three-dimensional intensity distribution. (b) Normalized intensity distribution of the lenses in the xy-focal plane on the left, and along the optical axis as an zy-plot. Intensity profiles in white are graphed through the center of the focus along the x-, y- and z-axis. Gaussian profiles are fitted to these profiles and shown in light red. See Table 1 for the comparison of designed and measured FWHM values. Mind the different axis scaling.

the xy-focal plane with values from a FWHM of 2.64 µm in x- and 2.52 µm in y-direction for the 0.15 NA lens (design 2.06 µm) to a FWHM of 1.01 µm in x- and 0.99 µm in y-direction for the 0.60 NA lens (design 0.52 µm). The better focusing performance of the higher NA lenses is especially visible when looking at the intensity distribution in the zy-plane plotted on the right

Optics EXPRESS

column of Fig. 2(b). Here, the FWHM along the optical axis is 53.78 µm for the 0.15 NA lens, decreasing to 7.65 µm for the 0.60 NA lens. See Table 1 for the comparison of designed and measured FWHM values for all four singlet diffractive lens types. The focusing performance of the diffractive singlets is close to the designed values. The deviations, however, increase with the NA of the singlets. This leads us to assume, that the fabrication resolution and tolerances are the likely culprit of the reduced optical performance. At high spatial frequencies of the diffractive elements, the lateral voxels dimensions in fabrication approach the feature size and period of the outer Fresnel zones.

Table 1. Full width at half maximum spot dimensions in lateral (denoted by the subscripts *xy*, *x*, and *y*) and axial direction (denoted by the subscript *z*) for the four diffractive singlet lenses. We give the designed as well as measured values, as extracted from Gaussian fits seen in Fig. 2.

	design (µm)		measured (µm)		
NA	$FWHM_{xy}$	$FWHM_z$	$FWHM_x$	$FWHM_y$	$FWHM_z$
0.15	2.06	47.73	2.64	2.52	53.78
0.30	1.03	11.72	1.28	1.28	14.84
0.45	0.68	5.05	1.05	1.01	8.41
0.60	0.52	2.70	1.01	0.99	7.65

3. Doublet diffractive stack for imaging

For imaging optics, the system requires a more advanced optical design. We achieve better performance at off-axis light fields, by utilizing a second diffractive surface in the system, resulting in a doublet diffractive lens stack, graphed schematically on the right of Fig. 1(a). Typically, at least one of the lenses of a 3D printed optical doublet needs to be anchored to the substrate or fiber by a supporting structure. This is the case both for refractive [17,21], and diffractive lens stacks [24,27]. Additionally, the supporting structure has to have openings to give the liquid resist room to dissolve into the developing solution. Printing lens stacks in porous media, such as the porous SiO_2, there is no need for a supporting structure, as the lenses are held in place by the porous media itself and the developing solution can penetrate through the pores of the medium. This allows for a faster and more feasible fabrication of strongly overhanging or even free-floating structures. Moreover, the optically active area for arrays of lens stacks can be as large as 100%. A top view microscope image of optical doublets is depicted in Fig. 1(b).

3.1. Optical design

The design of the diffractive doublet lens system is illustrated in Fig. 3. As design parameters we choose a wavelength of 633 nm, an aperture diameter of 550 µm, an optical diameter of 575 µm, and a physical diameter of 600 µm. At the design wavelength of 633 nm, the polymerized IP-n162 inside the $PSiO_2$ has a refractive index of 1.5687. We place the top diffractive lens 5 µm inside of the 60 µm thick $PSiO_2$ film and the bottom lens 45 µm below the top lens. With a working distance of 1000 µm in air, the diffractive doublet boasts an effective focal length of 1032 µm which result in an f# of 1.86 and an NA of 0.258. The modulation transfer function (MTF) of the diffractive doublet is plotted in Fig. 5, and discussed below. To achieve a field of view of roughly 20°, three ray fields at 0°, 5°, and 10° are implemented. We optimize the two diffractive lenses in Zemax OpticStudio 20.1, where they are defined by Eq. (1). The performance of the diffractive doublet is diffraction limited for field angles below about 3°, after which astigmatism, spherical aberrations and coma reduce the optical performance as is visible in the MTF shown in Fig. 5. The optimized parameters give a maximum spatial frequency of circa 201 mm^{-1} for the bottom

Optics EXPRESS

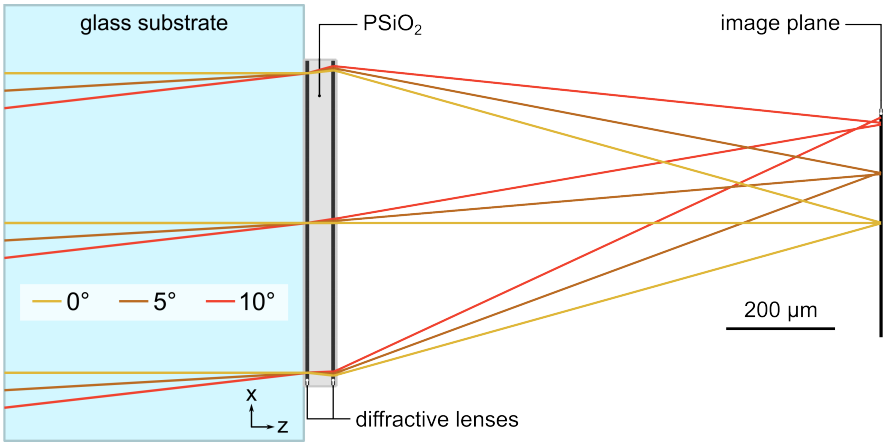

Fig. 3. Ray-optical design of a diffractive imaging doublet in a 60 µm thick $PSiO_2$ film with a diameter of 600 µm and focal length of 1 mm. The diffractive lenses are spaced 45 µm apart from each other.

and 639 mm^{-1} for the top lens. Both diffractive surfaces can thereby be fabricated easier than the singlet 0.45 NA and 0.60 NA lenses, which both have higher maximum spatial frequencies. The diffractive lens doublet is manufactured with the same technique as described above. Multiple doublets are shown in the right two columns of Fig. 1(b).

3.2. *Imaging performance*

To examine the optical performance of the doublet diffractive stack, we take images of an USAF 1951 resolution test chart at several magnifications. The basic setup is depicted in Fig. 4(a) and was previously utilized in [6,21]. Collimated white LED light (Thorlabs MCWHLP1 and Thorlabs AC254-040-A) first strikes a diffusor (Thorlabs DG10-1500-A) before being optically filtered using a band-pass filter. The filter is centered at 633 nm with a spectral FWHM of 10 nm (Thorlabs FL05632.8-10). The light is subsequently focused through a 10x magnification microscope objective (Mitutoyo M Plan Apo HR 10x, part number 378-788-4) and illuminates the USAF 1951 resolution test chart (Edmund Optics USAF HI-RES Target 2IN SQ NEG) before it strikes the diffractive doublet stack. We change the beam diameter in front of the first microscope objective with an iris (Thorlabs SM1D12C) to match the designed aperture of the diffractive doublet lens. The image is then analyzed by a basic microscopy setup in order to soley investigate the doublet system under test and not introduce pixilation, caused by direct imaging onto a camera. The microscopy setup consists of a 20x magnification microscope objective (Mitutoyo M Plan Apo 20x, part number 378-804-3), a tube lens and a camera (iDS UI-3180CP-C-HQ R2.1). We increase the magnification by reducing the distance between the USAF 1951 resolution test chart and the diffractive lens stack as well as centering on the relevant groups. Three different magnifications are illustrated in Fig. 4(b) through (d). The images show high contrast and quality throughout the groups. Some slight vignetting is visible at the edge of the higher elements of group 2 in Fig. 4(b), as well as some field curvature that is apparent at the edge of the image, visible in Fig. 4(c). Group 6 and 7 illustrated in Fig. 4(d) shows a slightly higher background intensity and therefore reduced contrast compared to the images in Fig. 4(b) and (c), which could be caused by light scattering at the various interfaces and in the porous medium itself. We quantify the resolution through the contrast, defined as

$$\text{contrast} = \frac{I_{\max} - I_{\min}}{I_{\max} + I_{\min}}. \tag{2}$$

Optics EXPRESS

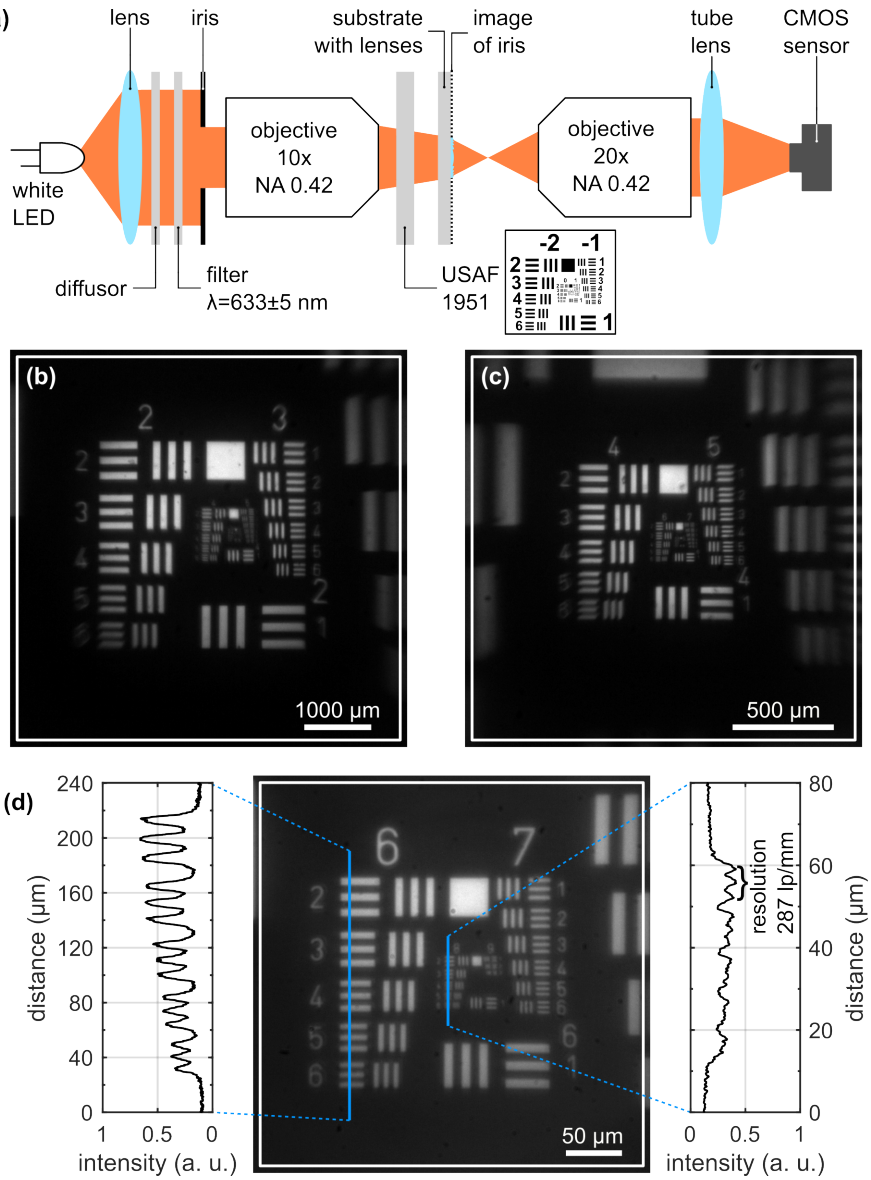

Fig. 4. Imaging performance of the diffractive doublet lens shown in Fig. 3. (a) Setup as previously shown in [21]. (b)-(d) Imaging of USAF 1951 resolution test charts at different magnifications, showing group 2 and 3 (b), group 4 and 5 (c), as well as group 6 and 7 (d). Intensity profiles of group 6 and 8, elements 2 to 6 are shown on the left and right of the image, where a resolution of group 8, element 2 is still possible with contrast higher than 10%. The scaling represents the size of the object.

With a resolution limit of 10%, the diffractive doublet stack is able to resolve element 2 of group 8, corresponding to a resolution of 287 lp /mm. Groups 6 and lower can be resolved clearly with higher contrast, which is plotted in the intensity profile in the left of Fig. 4(d). Taking the contrast for groups 2 to 8 of the USAF 1951 resolution test chart using the intensity levels depicted in Fig. 4(b) to (d), we construct the MTF, graphed in Fig. 5 for one diffractive doublet system. We then compare it to the design at the three different fields, 0°, 5° and 10° as well as

Optics EXPRESS

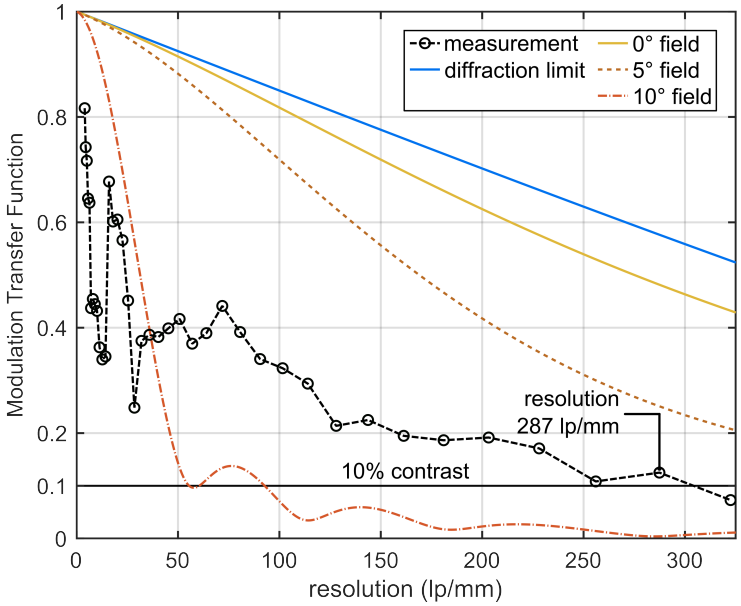

Fig. 5. Modulation Transfer Function (MTF) of the diffractive doublet. Each measured point corresponds to the contrast, defined by Eq. (2), of one element from the USAF 1951 resolution test chart, going from group 2, element 1 to group 8, element 3. The contrast exceeds 10% for a resolution of up to 287 lp /mm. The designed MTF is shown for the tangential rays at field angles of 0°, 5° and 10°, as shown in Fig. 3. While a wavelength of 633 ± 5 nm is used to measure the MTF of the doublet, the diffraction limit and MTF at field angles of the design are given for a wavelength of 633 nm.

giving the theoretical diffraction limit, also plotted in Fig. 5. The MTF of the diffractive doublet lens exhibits some oscillations in the lower frequencies. This could be owed to the fact, that the elements of the resolution test chart are imaged with different field angles and are prone to vignetting, which is visible in Fig. 4(b). The contrast remains at above 20% for resolutions up to roughly 160 lp /mm and above 10% for up to 287 lp /mm. All but the measured MTF are calculated for monochromatic light at 633 nm. Polychromatic light, even for the narrow bandpass filter spectral range of 633 ± 5 nm, reduces the designed MTF. A study on achromatic doublet microoptical systems in $PSiO_2$ is given in [23].

4. Fabrication

4.1. Sample preparation

A thorough description of the porousification of the silicon via etching as well as its thermal oxidation and transfer is given in [22,23]. The transferred film of $PSiO_2$ is visible as the ragged film on top of the glass substrate, as seen in Fig. 1(b). The average pore size of $PSiO_2$ produced by this method is 60 nm, which minimizes light scattering in the visible and infrared regions [22]. After transferring $PSiO_2$ onto quartz, the average total transmission (from 450 nm to 800 nm) increases from 95.6% (quartz only) to 97.2% due to the antireflection effect. This indicates that visible light perceives $PSiO_2$ as a homogeneous, transparent material, and the pores do not negatively affect the optical performance of the lenses printed within. Small cracks can develop during film transfer or the fabrication and developing process as described below, which can be seen on the right side of the sample. To prepare the sample for printing, the $PSiO_2$-film is infilled with the photoresist IP-n162 over night. While not utilized in this study, infilling of the

Optics EXPRESS

photoresist can be accelerated by placing the samples on a hot plate at 55-60°C for 3-5 minutes [19], and can be further accelerated by applying a lower than ambient pressure during the infilling process.

4.2. 3D printing in porous silicon oxide

All lenses are fabricated using by the commercially available 3D printer Nanoscribe Quantum X (Nanoscribe GmbH & Co. KG) using two-photon polymerization grayscale lithography (2GL). The photoresist is polymerized by a femtosecond pulsed laser at a central wavelength of 780 nm. The lenses are fabricated in the dip-in mode with the medium feature set consisting of a 25x magnification objective with an NA of 0.8 (LCI Plan-Neofluar 25x/0.8 Imm Korr DIC M27 420852-9973). This objective has a maximum calibrated writing field diameter of 700 µm. Larger structures can be fabricated by lower magnification objectives [6], usually at the cost of resolution, or by stitching together multiple writing fields. We utilize grayscale lithography to increase manufacturing throughput while achieving smoother structures [20,21]. During the 2GL fabrication, the laser power is modulated by an acousto-optical modulator instead of the constant power applied during the typical 2PP fabrication processes [6]. We utilize average powers between 0 mW and 65 mW, dynamically changing the voxels size, resulting in step-free surfaces even at comparatively large slicing distances of 1 µm. We employ a hatching distance of 0.2 µm. The laser is scanned through the resist using a pair of Galvo mirrors at 70 mm s^{-1} for the singlet diffractive lenses and the top lens of the diffractive doublet. The bottom lens of the diffractive doublet is scanned slightly faster with a speed of 85 mm s^{-1}. These parameters result in fabrication times of about 2 minutes for the singlet and 4 minutes for the doublet lenses. Typical fabrication on glass substrates takes the same laser powers, slicing and hatching distances while using a faster scan speed of 200 mm s^{-1} [21], reducing the fabrication time in the $PSiO_2$ by a factor of two to three for the same fabrication volume. As discussed in [22], $PSiO_2$ is non-absorptive in the visible and near-infrared range and its far sub-wavelength pore size (averaging 60 nm in diameter) limits light scattering at visible and infrared frequencies. During printing, the pore is filled with liquid IP-n162, which has a refractive index closer to SiO_2 compared to air, further reducing the light scattering. Therefore, the porous medium won't compromise the resolution and repeatability. Following the polymerization of the print, the liquid photoresist is removed in a bath of mr-dev 600 (micro resist technology) inside an air-tight container at 40 °C for 5.5 h. The sample is subsequently placed into an isopropyl alcohol bath overnight and then critical point dried with in a fresh bath of isopropyl alcohol in a CO_2 critical point dryer (Leica EM CPD300). Typical drying with air or gaseous nitrogen is also possible but can cause cracks due to the capillary forces inside the small channels within the $PSiO_2$. After fabrication, the samples can be handled the same way as 3D printed microoptics on glass substrates.

5. Conclusion and outlook

We have successfully fabricated singlet and doublet diffractive lenses by grayscale lithography femtosecond 3D printing inside porous SiO_2. The singlet lenses with NAs of up to 0.60 illustrate high focusing performance and are rapidly fabricated due to the small spatial extent. We save fabrication time and design effort for the diffractive imaging lens stack by utilizing an approach that does not require any supporting structures. The fabrication time is further reduced by utilizing grayscale lithography, allowing large slicing distances while keeping the shape accuracy. We observe high contrast and low aberrated images of the diffractive lens stack and analyse the contrast MTF, which shows great resolution of up to 287 lp /mm at over 10% contrast.

In the future, optical performance could be increased further with a third lens element in thicker films of porous SiO_2 or higher NA writing objectives. The porous SiO_2 matrix can also be infilled with liquids, providing a way to change the optical capabilities of the system.

Optics EXPRESS

For applications in more extreme environments, e.g., a thin protection layer of Al_2O_3 could be applied using different methods. Additionally, future research could also investigate the impact of porosity levels of SiO_2 on optical performance. Furthermore, fabrication times can be reduced further with light-sheet 3D-microprinting [28] or printing via digital holography [29].

Funding. National Science Foundation (NSF) through the University of Illinois at Urbana-Champaign Materials Research Science and Engineering Center (DMR-2309037); HORIZON EUROPE European Research Council (3DPRINTEDOPTICS: 862549); HORIZON EUROPE European Innovation Council (IV-Lab: 101115545); Deutsche Forschungsgemeinschaft (DFG-UP31/1, 431314977/GRK 2642); Bundesministerium für Bildung und Forschung (Integrated3DPrint 13N16874, PRINTOPTICS, QLink.X, QR.X); Ministerium für Wissenschaft, Forschung und Kunst Baden-Württemberg (Innovation Campus Future Mobility: SdManu1, Lab7); Baden-Württemberg Stiftung (OPTERIAL); Carl-Zeiss-Stiftung (Center Qphoton, EndoPrint3D).

Acknowledgments. The authors thank Rainer Stöhr for help with the CO_2 critical point drying.

Disclosures. The authors declare no conflicts of interest.

Data availability. Data underlying the results presented in this paper are not publicly available at this time but may be obtained from the authors upon reasonable request.

References

1. D. Gonzalez-Hernandez, S. Varapnickas, A. Bertoncini, *et al.*, "Micro-optics 3d printed via multi-photon laser lithography," Adv. Opt. Mater. **11**(1), 2201701 (2023).
2. Y. Zhu, T. Tang, S. Zhao, *et al.*, "Recent advancements and applications in 3d printing of functional optics," Addit. Manuf. **52**, 102682 (2022).
3. S. Wang, L. Kong, C. Wang, *et al.*, "Ultra-precision manufacturing of microlens arrays using an optimum machining process chain," Opt. Express **31**(2), 2234–2247 (2023).
4. M. Malinauskas, A. Žukauskas, K. Belazaras, *et al.*, "Laser fabrication of various polymer microoptical components," Eur. Phys. J. Appl. Phys. **58**(2), 20501 (2012).
5. T. Gissibl, S. Thiele, A. Herkommer, *et al.*, "Two-photon direct laser writing of ultracompact multi-lens objectives," Nat. Photonics **10**(8), 554–560 (2016).
6. S. Ristok, S. Thiele, A. Toulouse, *et al.*, "Stitching-free 3d printing of millimeter-sized highly transparent spherical and aspherical optical components," Opt. Mater. Express **10**(10), 2370–2378 (2020).
7. S. Schmidt, S. Thiele, A. Toulouse, *et al.*, "Tailored micro-optical freeform holograms for integrated complex beam shaping," Optica **7**(10), 1279–1286 (2020).
8. R. O. kedem, N. Opatovski, D. Xiao, *et al.*, "Near index matching enables solid diffractive optical element fabrication via additive manufacturing," Light: Sci. Appl. **12**(1), 222 (2023).
9. H.-B. Sun, S. Matsuo, and H. Misawa, "Three-dimensional photonic crystal structures achieved with two-photon-absorption photopolymerization of resin," Appl. Phys. Lett. **74**(6), 786–788 (1999).
10. G. von Freymann, A. Ledermann, M. Thiel, *et al.*, "Three-dimensional nanostructures for photonics," Adv. Funct. Mater. **20**(7), 1038–1052 (2010).
11. A. Bertoncini and C. Liberale, "Polarization micro-optics: Circular polarization from a fresnel rhomb 3d printed on an optical fiber," IEEE Photonics Technol. Lett. **30**(21), 1882–1885 (2018).
12. M. Farsari and B. N. Chichkov, "Two-photon fabrication," Nat. Photonics **3**(8), 450–452 (2009).
13. J. Li, S. Thiele, R. W. Kirk, *et al.*, "3d-printed micro lens-in-lens for in vivo multimodal microendoscopy," Small **18**(17), 2107032 (2022).
14. F. Lux, A. Calikoglu, C. Klusmann, *et al.*, "3d nanoprinted catadioptric fiber sensor for dual-axis distance measurement during vitrectomy," Appl. Opt. **63**(11), 2806 (2024).
15. L. Bremer, K. Weber, S. Fischbach, *et al.*, "Quantum dot single-photon emission coupled into single-mode fibers with 3d printed micro-objectives," APL Photonics **5**(10), 106101 (2020).
16. M. Sartison, K. Weber, S. Thiele, *et al.*, "3d printed micro-optics for quantum technology: Optimised coupling of single quantum dot emission into a single-mode fibre," Light: Adv. Manufact. **2**(2), 103 (2021).
17. D. Galvez, Z. Hong, A. D. Rocha, *et al.*, "Characterizing close-focus lenses for microendoscopy," J. Optical Microsystems **3**(01), 11003 (2023).
18. Y. Xu, P. Maier, M. Trappen, *et al.*, "3d-printed facet-attached microlenses for advanced photonic system assembly," Light: Sci. Appl. **12**(1), 1 (2023).
19. A. J. Littlefield, J. Huang, M. L. Holley, *et al.*, "Low loss fiber-coupled volumetric interconnects fabricated via direct laser writing," Optica **11**(7), 995 (2024).
20. T. Aderneuer, O. Fernández, and R. Ferrini, "Two-photon grayscale lithography for free-form micro-optical arrays," Opt. Express **29**(24), 39511 (2021).
21. L. Siegle, S. Ristok, and H. Giessen, "Complex aspherical singlet and doublet microoptics by grayscale 3d printing," Opt. Express **31**(3), 4179–4189 (2023).
22. C. R. Ocier, C. A. Richards, D. A. Bacon-Brown, *et al.*, "Direct laser writing of volumetric gradient index lenses and waveguides," Light: Sci. Appl. **9**(1), 196 (2020).

Optics EXPRESS

23. C. A. Richards, C. R. Ocier, D. Xie, *et al.*, "Hybrid achromatic microlenses with high numerical apertures and focusing efficiencies across the visible," Nat. Commun. **14**(1), 3119 (2023).
24. S. Thiele, C. Pruss, A. M. Herkommer, *et al.*, "3d printed stacked diffractive microlenses," Opt. Express **27**(24), 35621–35630 (2019).
25. V. A. Markel, "Introduction to the maxwell garnett approximation: tutorial," J. Opt. Soc. Am. A **33**(7), 1244 (2016).
26. M. Schmid, D. Ludescher, and H. Giessen, "Optical properties of photoresists for femtosecond 3d printing: refractive index, extinction, luminescence-dose dependence, aging, heat treatment and comparison between 1-photon and 2-photon exposure," Opt. Mater. Express **9**(12), 4564–4577 (2019).
27. A. Asadollahbaik, S. Thiele, K. Weber, *et al.*, "Highly efficient dual-fiber optical trapping with 3d printed diffractive fresnel lenses," ACS Photonics **7**(1), 88–97 (2020).
28. V. Hahn, P. Rietz, F. Hermann, *et al.*, "Light-sheet 3D microprinting via two-colour two-step absorption," Nature Photonics **16**, 784–791 (2022).
29. W. Ouyang, X. Xu, W. Lu, *et al.*, "Ultrafast 3d nanofabrication via digital holography," Nat. Commun. **14**(1), 1716 (2023).